Available online at www.sciencedirect.com
ScienceDirect
Ceramics International 37 (2011) 3651–3656
CERAMICS INTERNATIONAL
www.elsevier.com/locate/ceramint

Analysis of structural, thermal and dielectric properties of $LiTi_2(PO_4)_3$ ceramic powders

R. Ramaraghavulu *, S. Buddhudu

Department of Physics, Sri Venkateswara University, Tirupati 517502, India

Received 23 March 2011; received in revised form 12 June 2011; accepted 14 June 2011
Available online 21 June 2011

Abstract

Lithium titanium phosphate ($LiTi_2(PO_4)_3$) ceramic powders have been prepared by a solid state reaction method at five different temperatures (800 °C, 900 °C, 1000 °C, 1100 °C and 1200 °C for 5 h each). The XRD profiles have shown that the sample sintered at 1100 °C (optimized) has displayed well-defined features. XRD peaks are in good agreement with the JCPDS Card No. 35-0754 confirming the *rhombohedral* structure in a space group of $R\bar{3}c$. The SEM images of the five samples sintered have been examined. EDAX and Raman spectra have been obtained for the $LiTi_2(PO_4)_3$ ceramic powder sintered at 1100 °C for analysis. Thermal properties for the as prepared precursor $LiTi_2(PO_4)_3$ sample, have been analyzed from the TG-DTA profiles. Besides this, dielectric constant, dielectric loss and conductivities (σ_{ac} and σ_{dc}) have also been studied for the $LiTi_2(PO_4)_3$ ceramic powder.

Keywords: $LiTi_2(PO_4)_3$ ceramics; Characterization

1. Introduction

In recent times, interest has been evinced in phosphate compounds as insertion materials for lithium-ion batteries for different studies. A typical example of it, is a phosphate based $LiM_2(PO_4)_3$ [M – Ti, V, Fe, Zr] possessing NASICON (acronym for Na superionic conductor) type structure [1–5]. The crystal NASICON structure consists of a three dimensional network in which MO_6 octahedra share all their corners with PO_4 tetrahedra [6–8]. The interstitial and conduction channels are generated along the *c*-axis, in which Li^+ could be found occupying interstitial sites [9,10].

Lithium titanium phosphate ($LiTi_2(PO_4)_3$) has been considered as an anode material with high discharge capacity [11]. Mostly, these ionic conductors have titanium as the major component, which can easily take part in the intercalation or deintercalation exhibiting appreciable electrical conductivity [12–15]. The capacity rating of such batteries depends strongly on the diffusion of Li^+ ions [16].

In literature, no detailed study has so far been carried out on the $LiTi_2(PO_4)_3$ ceramic powder, therefore the present work has been undertaken to investigate its structural, thermal and conductivities (σ_{ac} and σ_{dc}) at an optimized sintering temperature.

2. Experimental

NASICON structure $LiTi_2(PO_4)_3$ ceramic powders were obtained by employing a solid state reaction method as given below, using the chemicals of Li_2CO_3, TiO_2 and $NH_4H_2PO_4$:

$$0.5Li_2CO_3 + 2TiO_2 + 3NH_4H_2PO_4 \rightarrow LiTi_2(PO_4)_3 + 3NH_3 + 0.5CO_2 + 4.5H_2O$$

Stoichiometric quantities of precursor materials were finely powdered in an agate mortor using the acetone as the binder solvent for 2 h to obtain homogeneous mixture. Later it was transferred into a porcelain crucible for its gradual heating in an electric tubular furnace up to 600 °C for 2 h. As synthesized powder from the above reaction, it was in light block color, which indicates the presence of residual carbon. When it was heat-treated at 600 °C, the powder turned into white color, revealing the complete disappearance of the residual carbons

* Corresponding author. Tel.: +91 9704919432.
E-mail address: ramaraghavulu@yahoo.co.in (R. Ramaraghavulu).

0272-8842/$36.00
doi:10.1016/j.ceramint.2011.06.025

from the ceramic powder precursor. It was again finely powdered for 1 h in an agate mortor in obtaining them in the form of five pellets each in the dimension of 1 cm diameter and ~1.5 mm thickness. These pellets were collected into porcelain crucibles each separately for sintering at 800 °C, 900 °C, 1000 °C, 1100 °C and 1200 °C for 5 h, respectively.

For the as synthesized precursor sample, differential thermal analysis (DTA) and thermogravimetric analysis (TGA) were simultaneously measured in N_2 atmosphere at a heating rate of 10 °C/min on a Netzesch STA 409 Simultaneous Thermal analyzer. The sintered ceramic powders were used for their XRD profiles on a XPert PRO PANalytical diffractometer with Cu Kα line of λ = 1.5406 Å in the measuremental range of 2θ from 10° to 70° at the rate of 0.016° in step width. The crystallite size was calculated by using Scherrer's equation $D_{\text{crystallite}} = k\lambda/(\beta \cos\theta)$. Where D was the crystallite size, k was Scherrer's constant = 0.9, λ = 1.5406 Å (X-ray wavelength), and β was full width half maxima (FWHM) at diffraction angle 2θ. The density values of the $LiTi_2(PO_4)_3$ sintered pellets were measured at room temperature using the standard Archimedies' principle, with water as the immersion liquid on a METTLET TOLEDO XS105 DualRangeAnalytical Balance. For each of the samples, morphology was examined on a ZEISS EVO MA15 Scanning Electron Microscope. The elemental analysis was carried out only for the sintering optimized (1100 °C) sample on a EDS (INCA pentaFETx3) attachment to the SEM system. Raman spectrum was recorded on a Horiba JobinYvon HR800 spectrometer with 532 nm of the laser (second harmonic peak of Nd:YAG) as the source of the excitation in the range of 100–1500 cm^{-1} with a spectral resolution of 5 cm^{-1}.

The dielectric measurements were carried out on a Phase Sensitive Millimeter (PSM 1700) LCR meter in the frequency range from 100 kHz to1 MHz for the sintered sample coated with silver paste. Dielectric constant (ε') values of $LiTi_2(PO_4)_3$ were calculated from

$$\varepsilon' = \frac{Cd}{\varepsilon_o A}$$

where ε_o is permittivity in vacuum = 0.0885 pF/cm^2, C is the capacitance of the specimen, d is the sample thickness and A is the area of the specimen in cm^2. The ac conductivity of $LiTi_2(PO_4)_3$ was calculated from

$$\sigma_{ac} = \varepsilon' \varepsilon_o \omega \tan\delta \ \ (\text{S cm}^{-1})$$

where ε_o is the permittivity in vacuum and ω is $2\pi f$ and tan δ is the dielectric loss. The dc conductivity was evaluated from the impedance spectroscopy measurement.

3. Results and discussion

Fig. 1 shows the TG/DTA profiles of the as synthesized precursor powder sample. From this figure we notice that there are two main weight losses in the TG curve, the first loss is located from the room temperature to 167 °C, with a total weight loss of 1.75% which is due to the evaporation of water

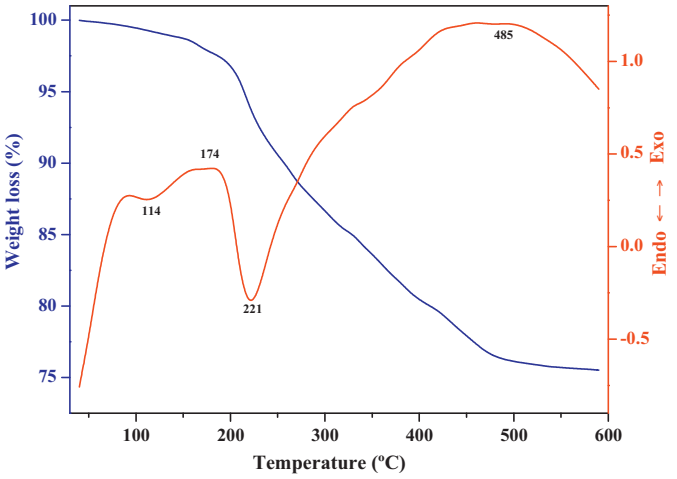

Fig. 1. TG–DTA profiles of the as synthesized precursor $LiTi_2(PO_4)_3$ powder.

and it is supported by the DTA curve showing an exothermic peak at 175 °C. The second weight loss is about ~23% in the range from 167 °C to 485 °C indicating the evaporation of CO_2 and NH_3 gases and also residual organic compounds. The endothermic peak at 221 °C in DTA curve shows the decomposition of $NH_4H_2PO_4$. Formation of the $LiTi_2(PO_4)_3$ takes place at 500 °C and beyond which there is no weight loss in the TG curve. From the TG curve, it is realized that with such losses, the sample weight will be only 75.50% and it is found to be satisfactorily matching with the calculated value of 73.99%. The prevailing difference of 1.51% may be due to certain impurities in the precursor powder. A broad exothermic peak in the DTA curve at 485 °C shows the crystallization trend in $LiTi_2(PO_4)_3$ ceramic powder.

X-ray diffraction profiles of the $LiTi_2(PO_4)_3$ ceramic powders sintered at 800 °C, 900 °C, 1000 °C, 1100 °C and 1200 °C for 5 h are shown in Fig. 2. The samples sintered at 800 °C and 900 °C have exhibited three additional peaks, two

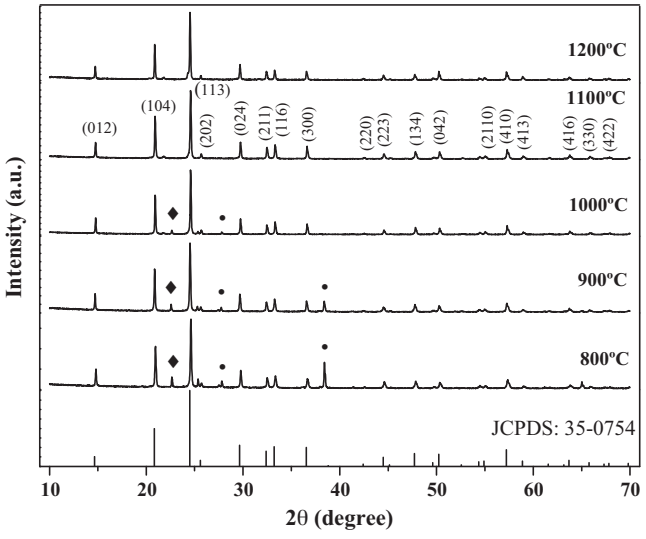

Fig. 2. X-ray diffraction profiles of $LiTi_2(PO_4)_3$ ceramic powders sintered at 800 °C, 900 °C, 1000 °C 1100 °C and1200 °C for 5 h and also the profile of the JCPDS Card No. 35-0754 of $LiTi_2(PO_4)_3$.

of which at $2\theta = 27.71^\circ$, 38.35° that are due to the TiO_2 [JCPDS Card No.79-1640] and the third peak at $2\theta = 22.71^\circ$ is because of TiP_2O_7 secondary phase [JCPDS Card No.38-1468]. These additional peaks are attributed to the impurities formed in the chemical reaction process at the time of grinding and sintering:

$$2LiTi_2(PO_4)_3 \rightarrow 3TiP_2O_7 + TiO_2 + Li_2O$$

$$TiP_2O_7 \rightarrow TiO_2 + P_2O_5$$

TiP_2O_7 and TiO_2 peaks appear in the XRD profiles up to 1000 °C but there are no Li_2O and P_2O_5 peaks because of their low melting temperatures and also their very limited presence will disappear in the sintering process at higher temperatures. Upon further increasing the sintering temperature, TiP_2O_7 and TiO_2 reflections would become disappeared at 1100 °C and above. If any further increase in the sintering temperature, it is noticed that the $LiTi_2(PO_4)_3$ reflections are decreasing and however the crystallite sizes are increasing. $LiTi_2(PO_4)_3$ ceramic powder sintered at 1100 °C related XRD Profiles are found to be in good agreement with the JCPDS card No 35-0754, structure in *Rhombohedral* with a space group of: $R\bar{3}c$. The lattice constants are $a = 8.5128$, $c = 20.878$ and $C = 2.4525$. The JCPDS profiles are shown in Fig. 2. The average crystallite size of the $LiTi_2(PO_4)_3$ ceramic powders at 800 °C, 900 °C, 1000 °C, 1100 °C and 1200 °C are calculated using Scherrer's equation $D_{crystallite} = k\lambda/(\beta \cos\theta)$ shown in Fig. 3. The crystallite sizes 73 nm, 70 nm, 86 nm, 78 nm and 80 nm corresponding sintering temperatures at 800 °C, 900 °C, 1000 °C, 1100 °C and 1200 °C for 5 h. Fig. 4(a) shows the bulk density of sintered $LiTi_2(PO_4)_3$, 2.72 g/cm^3, 2.72 g/cm^3, 2.64 g/cm^3, 2.69 g/cm^3 and 2.73 g/cm^3 at 800 °C, 900 °C, 1000 °C, 1100 °C and 1200 °C for each 5 h. Theoretical density of the $LiTi_2(PO_4)_3$ is 2.948 g/cm^3 [JCPDS card No 35-0754]. The relative densities of the sintered samples are shown in Fig. 4(b), showing 92.60%, 91.35%, 89.55%, 92.26% and 92.29% at 800 °C, 900 °C, 1000 °C, 1100 °C and 1200 °C correspond to the sintering temperatures. The density higher at powders sintered at 800 °C and 900 °C due the $LiTi_2O_7$ density is more (3.014 g/cm^3) [JCPDS card No: 38-14168] compare to $LiTi_2(PO_4)_3$ powders (2.948 g/cm^3). If temperature increases, amount of $LiTi_2O_7$ phase could be found decreased at 1000 °C. This may be due to a low density of $LiTi_2(PO_4)_3$ sintering temperature at 1000 °C. After 1000 °C, density increases due to the reduction in the grain boundaries.

Fig. 5(a)–(e) shows the microstructures of the $LiTi_2(PO_4)_3$ ceramic powders sintered at 800 °C, 900 °C, 1000 °C, 1100 °C and 1200 °C with changes in the grain sizes with an increase in sintering temperatures. Fig. 6 shows the EDS elemental analysis of the ceramic powder sintered at 1100 °C. The EDS of the sample could not display the presence of lithium because of its light weight as has been observed earlier by others [17,18]. The impurity of Al was to be found in (0.72%) from the EDAX analysis of $LiTi_2(PO_4)_3$ shows this Al impurity presence in TiO_2. It also shows the presence of O_2, P and Ti.

Fig. 7 shows the Raman spectrum of the $LiTi_2(PO_4)_3$ displaying P–O stretching vibrations in the region of

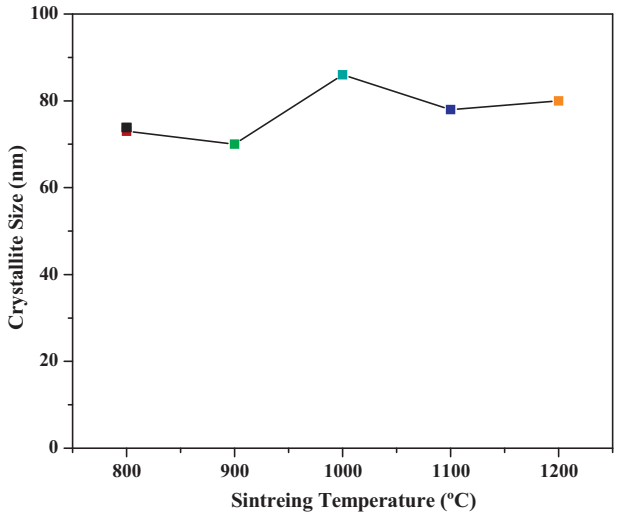

Fig. 3. Variation of crystallite sizes with the change in the sintering temperature.

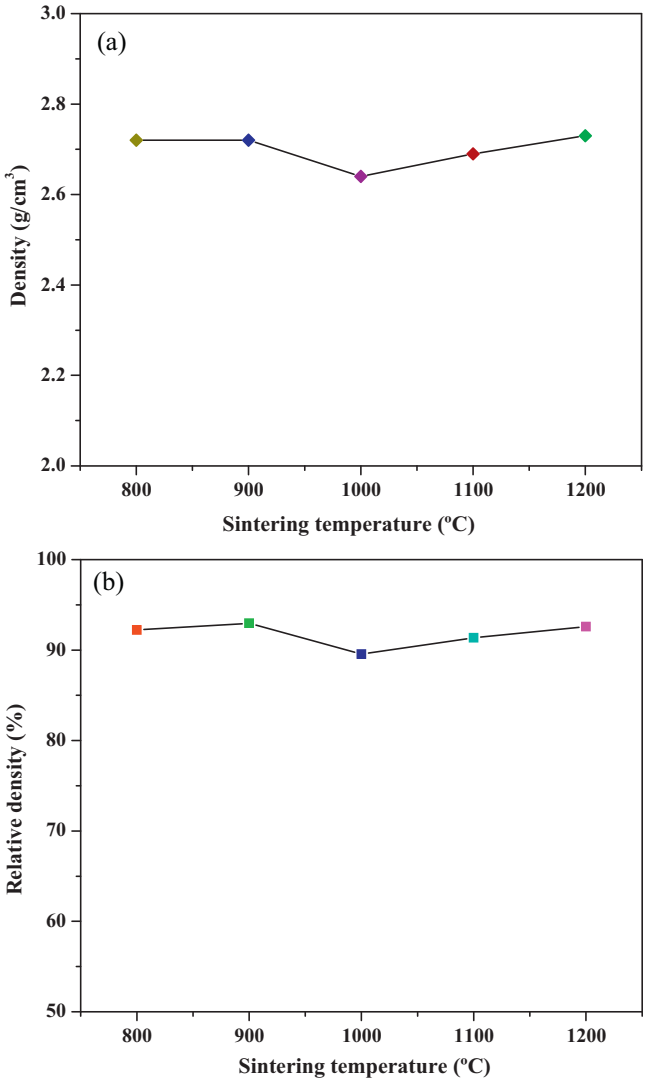

Fig. 4. (a) Variation of bulk density with the change in the sintering temperature. (b) Variation of relative density with the change in the sintering temperature.

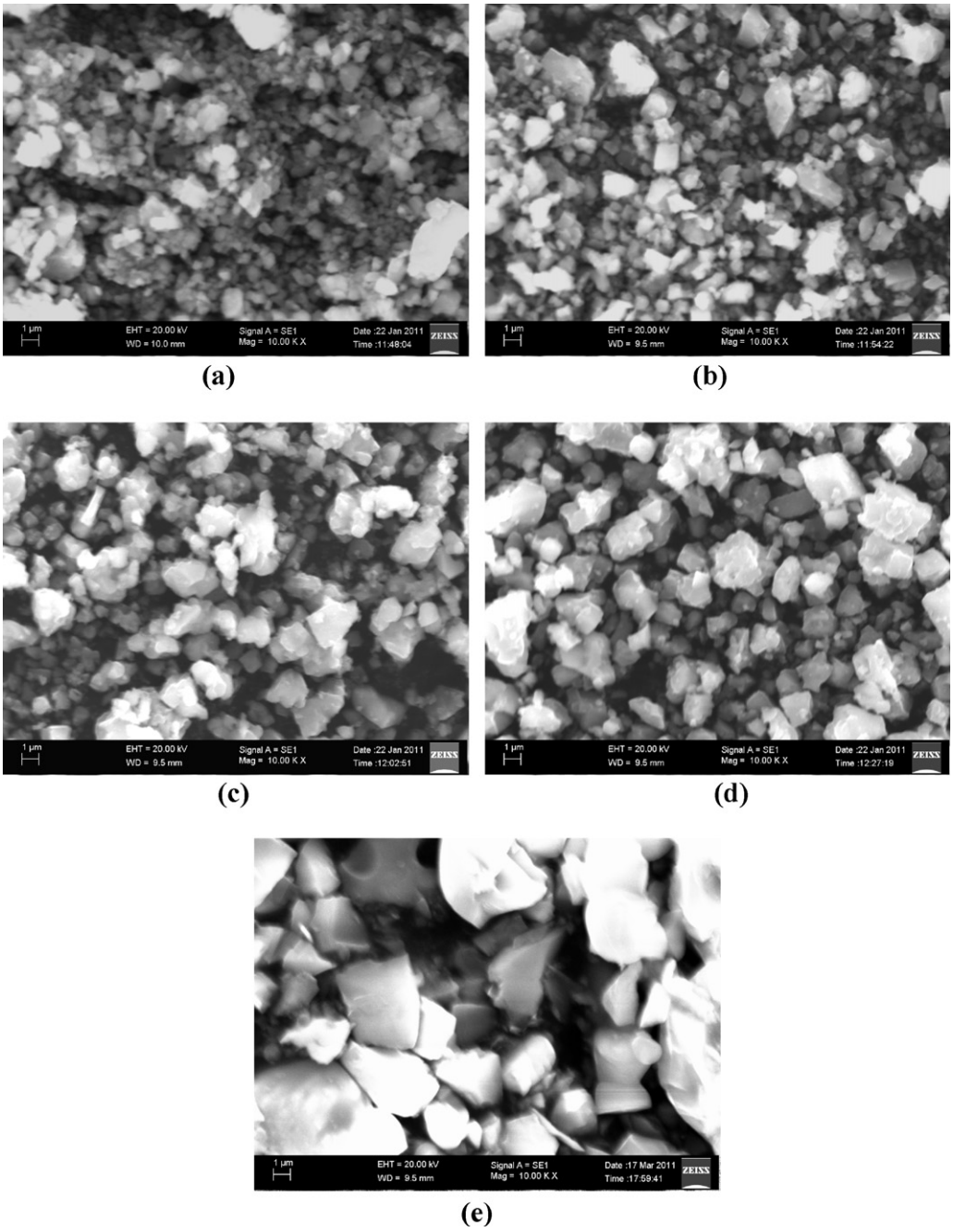

Fig. 5. SEM images of the $LiTi_2(PO_4)_3$ ceramic powders sintered at: (a) 800 °C, (b) 900 °C, (c) 1000 °C, (d) 1100 °C, and (e) 1200 °C.

900–1100 cm^{-1}. In general, the asymmetrical modes are at higher wavenumbers than the symmetrical ones. Raman bands assigned at 1098 cm^{-1} and 1007 cm^{-1} are the asymmetrical vibrations of $(PO_4)^{3-}$. The symmetrical bending vibration of PO_4^{3-} unit band located at 446 cm^{-1} [19,20]. The band at 280 cm^{-1} is assigned to translational vibration of the Ti^{4+} ions, while the bands at 355 cm^{-1}, 314 cm^{-1}, 240 cm^{-1} and 187 cm^{-1} are assigned to modes that predominantly contain PO_4^{3-} motions [21].

Fig. 8 shows the profiles of dielectric constant and dielectric loss in the frequency range of 100 kHz to 1 MHz for the $LiTi_2(PO_4)_3$ ceramic powder sintered at 1100 °C for 5 h. Decreasing nature of dielectric constant and dielectric loss with the increasing frequency may be due to relaxation behavior of the material [22]. The complex impedance spectrum (Z' vs. Z'') has been analyzed using Cole–Cole plots (Fig. 9) of the $LiTi_2(PO_4)_3$ ceramic powder. A single semicircular arc has been observed in a wide frequency range and this indicates that the electrical properties of the material could arise mainly due to the bulk effects [23]. The dc conductivity of the $LiTi_2(PO_4)_3$ ceramic powder has been determined from the bulk resistance (the diameter of the semicircle) and geometrical factors (the thickness and the electrode area) using the formula $\sigma_{dc} = d/(R_bA)$ [24]. Where d is thickness of the electrode, R_b is the bulk resistance of the material and A is the area of the electrode. The calculated dc conductivity of the $LiTi_2(PO_4)_3$ is 1.83×10^{-6} S cm^{-1}. The

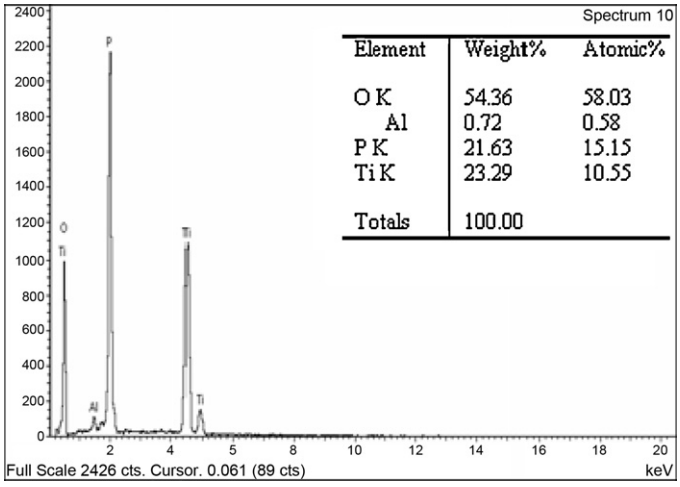

Fig. 6. EDAX profile of $LiTi_2(PO_4)_3$ powder sintered at 1100 °C.

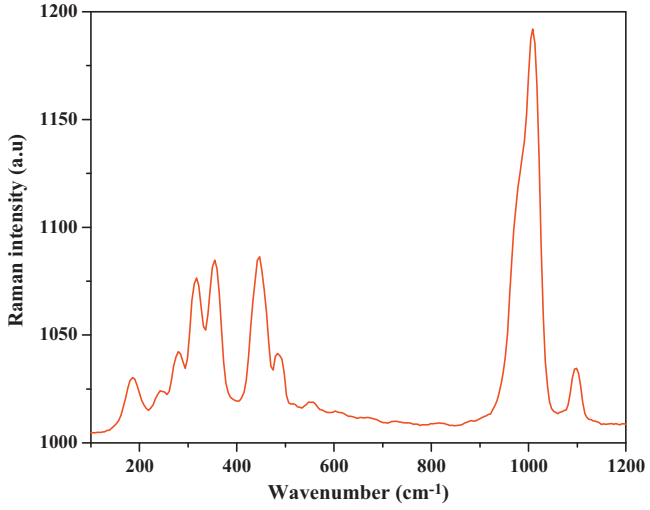

Fig. 7. Raman spectrum of $LiTi_2(PO_4)_3$ ceramic powders sintered at 1100 °C.

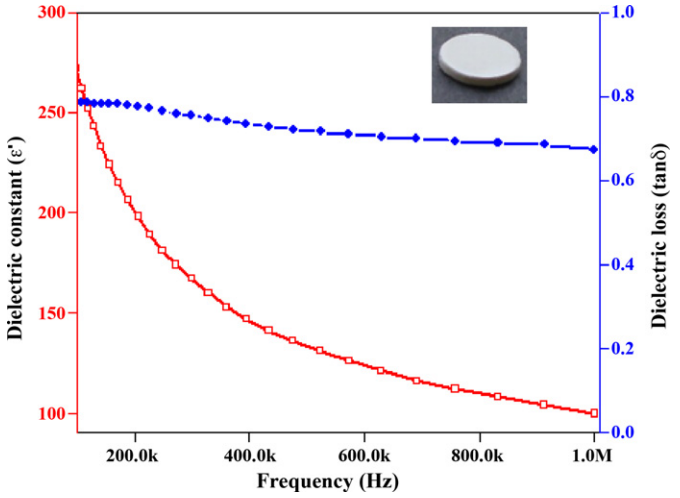

Fig. 8. Room temperature profiles of dielectric constant (ε') and dielectric loss (tan δ) of $LiTi_2(PO_4)_3$ sintered at 1100 °C as a function of the frequency change from 100 kHz to 1 MHz (inset fig shows a pellet form of $LiTi_2(PO_4)_3$ ceramic powder).

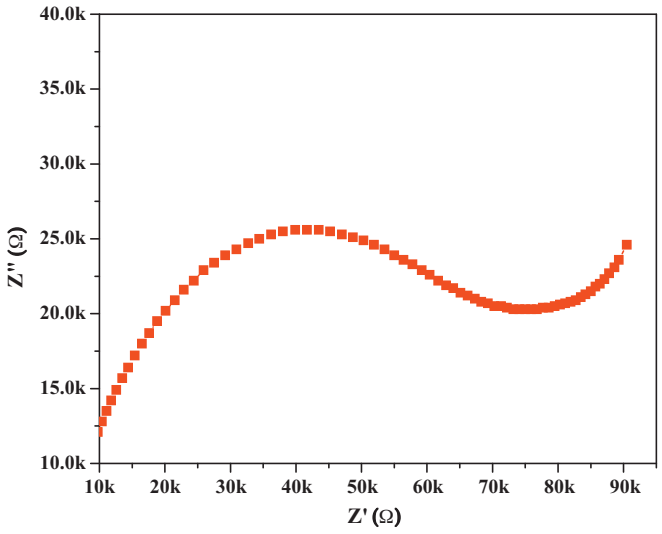

Fig. 9. Room temperature impedance spectrum of $LiTi_2(PO_4)_3$ pellet sintered at 1100 °C.

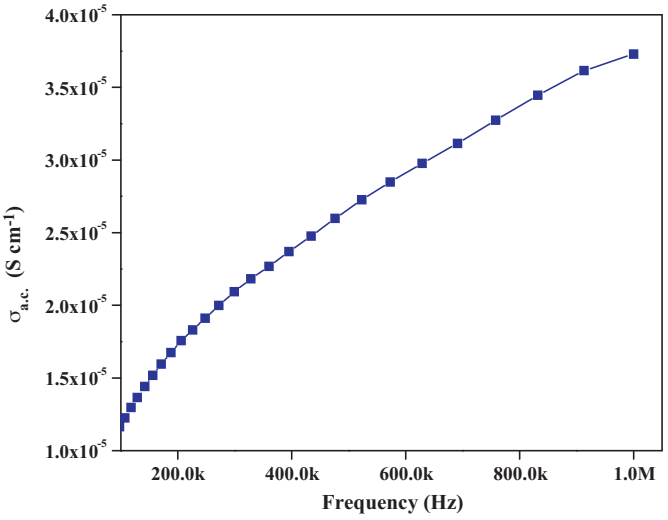

Fig. 10. Variation of ac conductivity (σ_{ac}) of $LiTi_2(PO_4)_3$ sintered at 1100 °C as function of frequency changes.

variation of ac conductivity (σ_{ac}) of the material is shown in Fig. 10. The ac conductivity (σ_{ac}) is 1.17×10^{-5} S cm^{-1} it is high compared to dc conductivity (σ_{dc}) 1.83×10^{-6} S cm^{-1} this is because of the fact that the dc conductivity originates due to the long range motion of the ions in the grains, on the other hand ac conductivity is due to the occurrence of the ionic motion in the shorter length scales. That is the reason why, the ac conductivity (σ_{ac}) is in higher value compared to the dc conductivity (σ_{dc}) [25].

4. Conclusion

$LiTi_2(PO_4)_3$ ceramic powders have successfully been prepared by a solid state reaction method at five different temperatures of 800 °C, 900 °C, 1000 °C, 1100 °C and 1200 °C. The sample sintered at 1100 °C (optimized temperature) has clearly exhibited a *rhombohedral* structure in space

group of $R\bar{3}c$ (based on the XRD features) which is in accordance with the JCPDS Card No. 35-0754. For the as synthesized precursor $LiTi_2(PO_4)_3$ powder, simultaneous TG-DTA profiles have been obtained and analyzed for studying their thermal properties. Raman spectrum of $LiTi_2(PO_4)_3$ ceramic powder sintered at 1100 °C has been analyzed. Besides those, its dielectric constant (ε'), dielectric loss (ε'') and dc conductivity (σ_{dc}), ac conductivity (σ_{ac}) properties have been have also been investigated.

References

[1] C. Delmas, A. Nadiri, J.L. Souberoox, The NASICON-type titanium phosphate $ATi_2(PO_4)_3$ (A = Li, Na) as electrode material, Solid State Ionics 28–30 (1988) 419–423.

[2] C.R. Mariappan, C. Galven, M.P. Crosnier-Lopez, F. Le Berre, O. Bohnke, Synthesis of nanostructured $LiTi_2(PO_4)_3$ powder by a Pechini-type polymerization complex method, J. Solid State Chem. 179 (2006) 450–456.

[3] M. Certin, H. Khirddine, P. Fabry, NASICON structure for alkaline ion recognition, Sens. Actuators B 43 (1997) 224–229.

[4] H. Wang, K. Huang, Y. Zeng, S. Yang, L. Chen, Electrochemical properties of TiP_2O_7 and $LiTi_2(PO_4)_3$ as anode material for lithium ion with aqueous solution electrolyte, Electrochim. Acta 52 (2007) 3280–3285.

[5] J. Wolfenstine, D. Foster, J. read, J.L. Allen, Rate-controlling species for the sintering of $LiTi_2(PO_4)_3$, J. Power Sources 182 (2008) 626–629.

[6] E. KAzakevicius, T. Salkus, A. Dindune, Z. Kanepe, J. Ronis, A. Keziionis, V. Kazlausliene, J. Miskinis, A. Selskiene, A. Selskis, La-doped $LiTi_2(PO_4)_3$ ceramics, Solid State Ionics 179 (2008) 51–56.

[7] H. Aono, E. Sugimoto, Y. Sadaoka, N. Imanaka, G.-Y. Adachi, Ionic conductivity and sinterability of lithium titanium phosphate system, Solid State Ionics 40/41 (1990) 38–42.

[8] A. Eljazouli, A. Nadiri, J.M. Dance, C. Delmas, G. Leflem, Relationships between structure magnetic properties of titanium(III) NASICON type phosphates, J. Phys. Chem. Solids 49 (1988) 779–783.

[9] L. Vijayan, G. Govindaraj, Impedance spectroscopic studies of planetary ball-milled lithium titanium phosphate material, Physica B 404 (2009) 3539–3543.

[10] P. Maldonado-Manso, M.C Martin-Sedeno, S. Bruque, J. Sanz, E.R. Losilla, Unexpected cationic distribution in tetrahedral/octahedral sites in nominal $Li_1 + xAl_xGe_{2-x}$ NASICON series, Solid State Ionics 178 (2007) 43–52.

[11] H. Noduchi, Secondary batteries-lithium rechargeable system-lithium-ion negative electrode: titanium-based materials, Encycl. Electrochem. Powder Sources (2009) 214–224.

[12] Y. Kobayashi, T. Rakeuchi, M. Tabuchi, K. Ado, H. Ageyama, Densification of $LiTi_2(PO_4)_3$-based solid electrolytes by spark-plasma-sintering, J. Power Sources 81–82 (1999) 853–858.

[13] N. Kosava, E. Devyatkia, On mechanical preparation of materials with enhanced characteristics for lithium batteries, Solid State Ionics 172 (2004) 181–184.

[14] G. Butt, N. Sammesb, G. Tompsett, A. Smirnova, O. Yamamotod, Raman spectroscopy of superionic Ti-doped $Li_3Fe(PO_4)_3$ and $LiNiPO_4$ structures, J. Power Sources 134 (2004) 72–79.

[15] G.X. Wang, D.H. Bradhurst, S.X. Dou, H.K. Liu, $LiTi_2(PO_4)_3$ with NASICON-type structure as lithium-storage materials, J. Power Sources 124 (2003) 231–236.

[16] X. Wu, Z. Wen, X. Xu, J. Han, Synthesis and ionic conductivity of Mg-doped Li_2TiO_3, Solid State Ionics 179 (2008) 1779–1782.

[17] A. Fini, G. Fazio, M.A. Holgado, M.J.F. Herva, Fractal and reactive dimensions of some ursodeoxycholic acid salts, Int. J. Pharm. 171 (1998) 45–52.

[18] Y. Kojima, K. Suzuki, Y. Kawai, Hydrogen generation from lithium borohydride solution over nano-sized platinum dispersed on $LiCoO_2$, J. Power Sources 155 (2006) 325–328.

[19] V.S. Kurazhkovskaya, D.M. Bykov, E.Y. Borovikova, N.Y. Boldyrev, L. Ikhalistsyn, A.I. Orlova, Vibrational spectra and factor group analysis of lanthanide zirconium phosphates $M^{III}_{0.33}Zr_2(PO_4)_3$, where M^{III} = Y, La-Lu, Vib. Spectrosc. 52 (2010) 137–143.

[20] R. Pikl, D. de Waal, A. Aatiq, A. El Jazouli, Vibrational spectra and factor group analysis of $Mn_{(0.5+x)}Ti_{(2-2x)}Cr_{2x}(PO_4)_3$ $\{0 \leq x \leq 0.50\}$, Vib. Spectrosc. (1998) 137–143.

[21] C.M. Burba, R. Frech, Vibrational spectroscopic study of lithium intercalation into $LiTi_2(PO_4)_3$, Solid State Ionics 177 (2006) 1489–1494.

[22] O.P. Nautiyal, S.C. Bhstt, R.P. Pant, B.S. Semwal, Dielectric properties of silver sodium niobate mixed ceramic system, Indian J. Pure Appl. Phys. 48 (2010) 357–362.

[23] B. Behera, P. Nayak, R.P.N. Choudhary, Dielectric and impedance properties of $LiCa_2Nb_5O_{15}$ ceramics, J. Mater. Sci: Mater. Electron. 19 (2008) 1005–1011.

[24] N. Ozer, C.M. Lampert, Electrochemical lithium insertion in sol-gel deposited $LiNbO_3$, Sol. Energy Mater. Sol. Cells 39 (1995) 367–375.

[25] Indris S S., Heitjans S P., M. Ulrich, A. Bunde, AC and DC conductivity in nano-and microcrystalline $LiO:B_2O_3$ composites: experimental results and theoretical models, Z. Phys. Chem. 219 (2005) 89–103.